Journal of Alloys and Compounds 509 (2011) 8664–8669

Contents lists available at ScienceDirect

Journal of Alloys and Compounds

journal homepage: www.elsevier.com/locate/jallcom

Processing, microstructure and mechanical properties of magnesium matrix nanocomposites fabricated by semisolid stirring assisted ultrasonic vibration

K.B. Nie, X.J. Wang*, K. Wu, L. Xu, M.Y. Zheng, X.S. Hu

School of Materials Science and Engineering, Harbin Institute of Technology, No. 92, West Da-Zhi Street, Harbin 150001, PR China

ARTICLE INFO

Article history:
Received 12 May 2011
Received in revised form 21 June 2011
Accepted 21 June 2011
Available online 28 June 2011

Keywords:
Magnesium matrix nanocomposite
Semisolid stirring
Ultrasonic vibration
Nanoparticle distribution
Grain refinement

ABSTRACT

Particulate reinforced magnesium matrix nanocomposites were fabricated by semisolid stirring assisted ultrasonic vibration. Compared with the as-cast AZ91 alloy, the grain size of matrix alloy in the SiCp/AZ91 nanocomposite stirring for 5 min was significantly decreased due to the addition of SiC nanoparticles. SiC nanoparticles within the grains exhibited homogeneous distribution although some SiC clusters still existed along the grain boundaries in the SiCp/AZ91 nanocomposite stirring for 5 min. With increasing the stirring time, agglomerates of SiC nanoparticles located along the grain boundaries increased. The ultimate tensile strength, yield strength and elongation to fracture of the SiCp/AZ91 nanocomposite stirring for 5 min were simultaneously improved compared with the as-cast AZ91 alloy. However, the ultimate tensile strength and elongation to fracture of the SiCp/AZ91 nanocomposite decreased with increasing the stirring time.

1. Introduction

Many efforts are under way to develop magnesium-based materials that have great potential as structural materials for the aerospace and automobile industries and offer significant weight savings targeted primarily for their further development [1,2]. However, the relatively low strength, poor room temperature ductility and toughness limit the range of magnesium applications [3]. As a result, magnesium matrix nanocomposites due to their low density and superior mechanical properties have fueled significantly research activities [4,5].

Processing technique is the key to fabrication of magnesium matrix nanocomposites with optimized properties. Stir casting that utilizes mechanical stirring is a widely used technique of producing magnesium matrix composites reinforced with micro ceramic particles. A combination of good distribution and dispersion of micro particles can be achieved by stir casting. However, it is extremely challenging for the conventional stir casting to distribute and disperse nanoparticles uniformly in magnesium melts because of their large surface-to-volume ratio and their low wettability in metal melts. In general, magnesium matrix nanocomposites are mostly made with expensive powder metallurgy, disintegrated melt deposition, friction stir processing, mechanical milling and ultrasonic vibration [6–17]. Another study on the synthesis and characterization of the $Mg_{65}Y_{10}Cu_{20}Ag_5$-based amorphous composite reinforced by ZrO_2 nanoparticles has shown improvements in hardness and distribution of nanoparticles in the matrix [18]. Among these processing techniques, ultrasonic vibration is efficient in dispersing nanoparticles in metal melts (including magnesium alloy) [15–17]. It was reported [19] that ultrasonic cavitation could produce transient (in the order of nanoseconds) micro "hot spots" that could have temperatures of about 5000 °C, pressures above 1000 atm, and heating and cooling rates above 10^{10} K/s. But it was a time-consuming process to introduce the nanoparticles into the magnesium melt through ultrasonic vibration as reported by Li et al. Thus, it is considered that the stir casting could be combined with ultrasonic vibration to produce magnesium matrix nanocomposite. Semisolid stirring can be utilized to incorporate the nanoparticles and disperse the nanoparticles macroscopically. And the strong impact coupled with local high temperatures introduced by ultrasonic vibration can break nanoparticle clusters and clean the nanoparticle surface from the view of microcosmic.

To the best of our knowledge, open literature reports so far suggested that no systematic attempt is made to fabricate the magnesium matrix nanocomposite by semisolid stirring assisted ultrasonic vibration. Accordingly, the experiments described in the present work were designed to examine the microstructure and mechanical properties of particulate reinforced magnesium matrix

* Corresponding author. Tel.: +86 45186402291; fax: +86 45186413922.
E-mail addresses: kaibo.nie@gmail.com (K.B. Nie), xjwang@hit.edu.cn (X.J. Wang).

0925-8388/$ – see front matter © 2011 Elsevier B.V. All rights reserved.
doi:10.1016/j.jallcom.2011.06.091

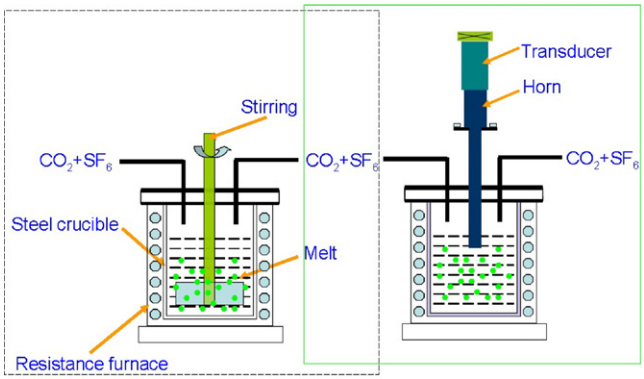

Fig. 1. Schematic of experimental setup for semisolid stirring assisted ultrasonic vibration of magnesium melt.

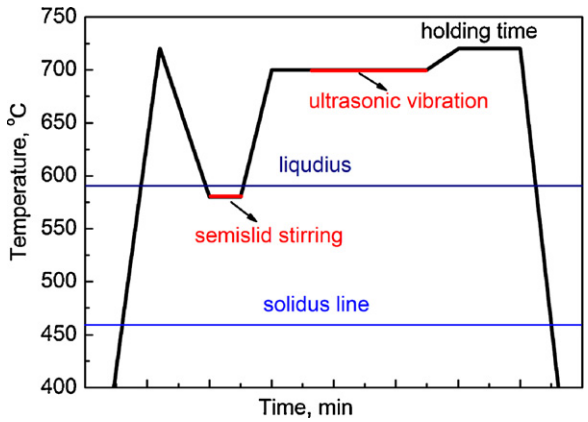

Fig. 2. Schematic illustration of the temperature–time sequences for semisolid stirring assisted ultrasonic vibration.

nanocomposites fabricated by semisolid stirring assisted ultrasonic vibration.

2. Experimental conditions

2.1. Materials

A commercial AZ91 alloy ingot (supplied by Northeast Light Alloy Company Limited, China) with a nominal composition of Mg–9.07Al–0.68Zn–0.21Mn was selected as the matrix alloy of the SiCp/AZ91 nanocomposite. SiC nanoparticles (supplied by Hefei Kaier Nanometer Energy & Technology Company Limited, China) with an average diameter of 60 nm were used as the reinforcement.

2.2. Preparation of materials

The experimental setup for semisolid stirring assisted ultrasonic vibration is given in Fig. 1. Fig. 2 gives a flow to show the whole fabrication process against temperature. First, about 1 kg of AZ91 alloy was melted at 720 °C under an atmosphere containing a gas mixture of CO_2/SF_6 and then cooled to 590 °C at which the matrix alloy was in semi-solid condition; SiC nanoparticles which were preheated to 550 °C were quickly added into the semi-solid alloy. The volume content of SiC nanoparticles in the SiCp/AZ91 nanocomposites was 1% while the stirring time for the SiCp/AZ91 nanocomposites was 5 min, 10 min and 25 min (ST5, ST10 and ST25), respectively.

After adequately stirring the melt, the melt was rapidly reheated to 700 °C and held at this temperature for 5 min. Then the ultrasonic probe was dipped into the melt for about 20 mm after the stirrer was removed from the melt. The ultrasonic vibration device consists of a transducer with a maximum power of 2 kW and frequency of about 20 kHz. The melt was ultrasonically processed for 20 min before the ultrasonic probe was removed. Then the melt was elevated to a pouring temperature of 720 °C and cast into a preheated steel mould (450 °C) and allowed to solidify under a 100 MPa pressure. It should be noted ultrasonic vibration was not used during the solidification process but in molten nanocomposite. For comparison, an AZ91 alloy ingot without semisolid stirring assisted ultrasonic vibration was also cast under the same conditions. Two ingots were cast for each condition.

2.3. Microstructural characterization

Optical microscopy (OM), scanning electron microscopy (SEM) and transmission electron microscopy (TEM) were used to study the microstructure modification of the matrix and reinforcement distribution in the SiCp/AZ91 nanocomposites intro-

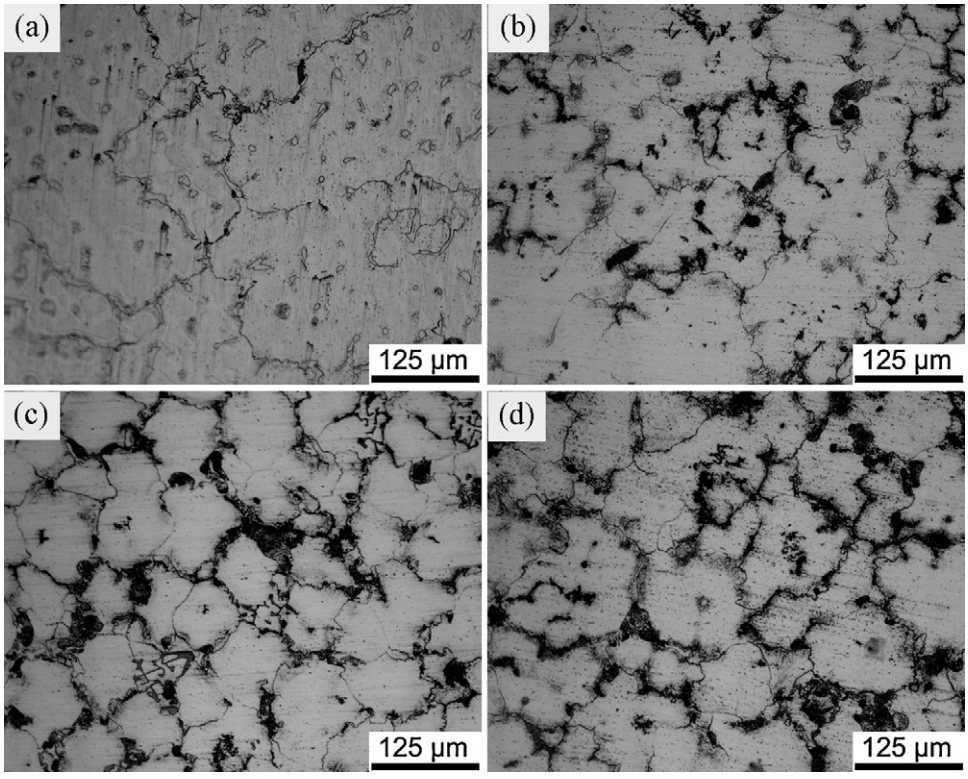

Fig. 3. OM micrographs of (a) AZ91 alloy; SiCp/AZ91 nanocomposites (b) stirring for 5 min; (c) stirring for 10 min; and (d) stirring for 25 min.

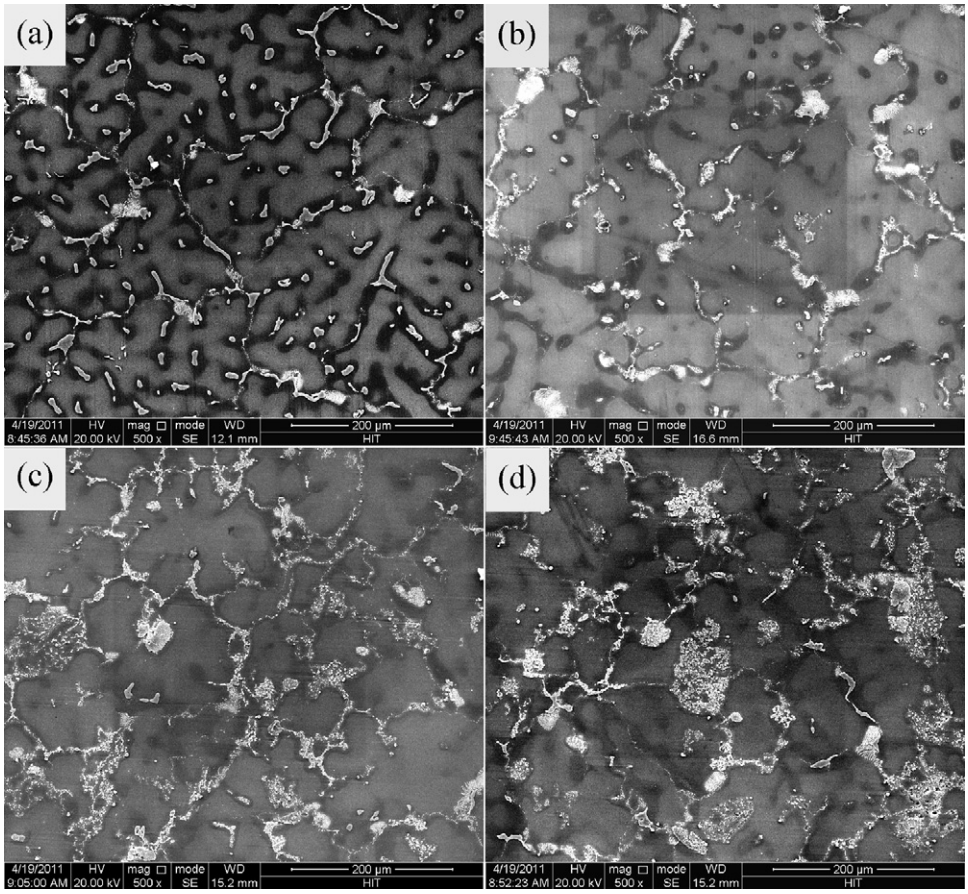

Fig. 4. SEM micrographs of (a) AZ91 alloy; SiCp/AZ91 nanocomposites (b) stirring for 5 min; (c) stirring for 10 min; and (d) stirring for 25 min.

ducing by semisolid stirring assisted ultrasonic vibration. Samples for OM and SEM were prepared by the conventional mechanical polishing and etching using 4% oxalic acid for 5–10 s. Microstructural features of the SiCp/AZ91 nanocomposites were identified using energy dispersive spectrophotometric (EDS) analysis. Specimens for TEM were prepared by grinding-polishing the sample to produce a foil of 50 μm thickness followed by punching 3 mm diameter disks. The disks were ion beam thinned.

2.4. Tensile test

Tensile test was carried out on an Instron Series 5569 test machine at room temperature with the tensile rate of 0.5 mm/min. Three samples for repeat tensile tests were cut from each ingot and the tensile strength reported in the work was averaged from the three tensile tests.

3. Results and discussion

3.1. Microstructures

Fig. 3 shows the OM micrographs of as-cast AZ91 alloy and SiCp/AZ91 nanocomposites. As shown in Fig. 3(a), the microstructure of the as-cast AZ91 alloy consists of primary α-Mg and eutectic phase β-$Mg_{17}Al_{12}$. The phase $Mg_{17}Al_{12}$ in the form of plates mainly locates at grain boundaries in the AZ91 alloy. The grains of the matrix alloy in the SiCp/AZ91 nanocomposites are refined as shown in Fig. 3(b)–(d), which suggests that the presence of SiC nanoparticle results in a much finer grain structure in as-cast AZ91 magnesium alloy. With extending the stirring time, the grain size of the matrix alloy in the SiCp/AZ91 nanocomposites changes not obviously.

Fig. 4 is the SEM micrographs of as-cast AZ91 alloy and the SiCp/AZ91 nanocomposites. From Fig. 4(a) it can be seen that most of the phase $Mg_{17}Al_{12}$ along grain boundaries in the as-cast AZ91 alloy are in the form of plates. This is consistent with the morphology of the phase $Mg_{17}Al_{12}$ as shown in Fig. 3(a). However, most of the phase $Mg_{17}Al_{12}$ in the SiCp/AZ91 nanocomposite stirring for 5 min is changed to fine and oriented lamellae due to the addition of SiC nanoparticles as shown in Fig. 4(b). With increasing the stirring time, as shown in Fig. 4(c) and (d), the amount of SiC nanoparticle clusters located at the grain boundaries increase which is in agreement with the nanoparticle cluster as shown in Fig. 3(c) and (d).

At higher magnification the morphology and distribution of SiC nanoparticles within the grains of matrix alloy in the SiCp/AZ91 nanocomposite stirring for 5 min are shown in Fig. 5(a). EDS of C K, Mg K and Si K (Fig. 5(b)–(d)) demonstrate that composition of the particle is SiC nanoparticles. The EDS of Si K is homogeneous which indicates that the distribution of SiC nanoparticle within the grains is uniform although some SiC nanoparticle clusters still exist.

Fig. 6 shows the TEM micrographs of SiC nanoparticles in the SiCp/AZ91 nanocomposites. The SiC nanoparticles exhibit homogeneous distribution in the SiCp/AZ91 nanocomposite stirring for 5 min as shown in Fig. 6(a) and (b). This indicates that semisolid stirring assisted ultrasonic vibration is effective in dispersing the nanoparticles in magnesium melt. With increasing the stirring time, some SiC nanoparticles are found to be agglomerated as shown in Fig. 6(c). This is in agreement with the particle cluster as shown in Fig. 4(c). At higher magnification, most of the SiC nanoparticles inside the cluster are still segregated by magnesium matrix as shown in Fig. 6(d).

The microstructure of nanocomposite usually depends on the nucleation stage and the subsequent growth condition. It is known that there are many submicroscopic particles of insoluble solid

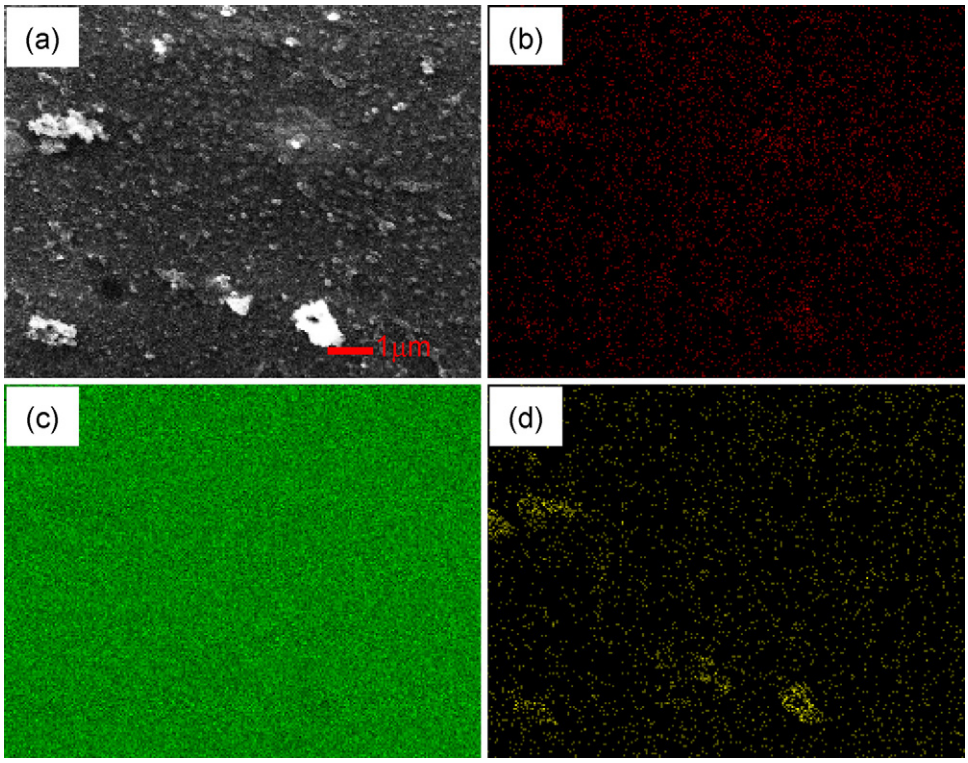

Fig. 5. SEM micrographs of (a) SiCp/AZ91 nanocomposite stirring for 5 min; EDS of (b) C K; (c) Mg K and (d) Si K.

impurities in the magnesium melt, but the number of active particles is insufficient for effective heterogeneous nucleation. In order to achieve the grain refinement of matrix alloy, the sufficient nuclei are essential [20,21]. In the present work, the SiC nanoparticles reinforced magnesium matrix nanocomposites were produced by semisolid stirring assisted ultrasonic vibration. During the ultrasonic vibration after semisolid stirring process, when the magnesium melt is subjected to local random compression-expansion cycles, if the local pressure in the melt becomes less than its vapor pressure during the half-period of expansion, an ultrasonic cavitation is formed. Since nanoparticle clusters are loosely packed together, air, inert gas, or metal vapor can be trapped inside the voids in the clusters to serve as nuclei for ultrasonic cavitations. The ultrasonic cavitations continue to grow until collapse during the half-period of compression, thus producing a high intensity shock wave in the melt [22]. Under the action of high intensity of shock, the insoluble solid impurities including SiC nanoparticles throughout the melt become active and involve in the solidification of process as nuclei, which lead to the heterogeneous nucleation easily upon a slight undercooling.

However, the final microstructure of nanocomposite is determined not only by the nucleation, but also by the growth condition. In the present processing condition, part of the initial nuclei introduced by ultrasonic cavitation may remelt when the SiCp/AZ91 nanocomposite melt is elevated to a pouring temperature of 720 °C after the ultrasonic probe is removed. Furthermore, the temperature of the steel mould for casting is high (450 °C) resulting in a slow extraction of latent heat during the later solidification process. In addition, the "push" effect of the solidification front on the insoluble solid impurities including nanoparticles may also cause the nuclei clusters along grain boundaries [23,24]. Thus, the grain refinement as well as the refined phase $Mg_{17}Al_{12}$ along the grain boundaries of the SiCp/AZ91 nanocomposites, as shown in Figs. 3 and 4, could be attributed to the combined effect of heterogeneous nucleation of primary magnesium on SiC particles and restricted growth of magnesium grains during solidification. However, with increasing the semisolid stirring time the viscosity of molten magnesium melt increases resulting in decrease of the effect of ultrasonic cavitation during the following ultrasonic vibration process. As a result, more agglomerates of SiC nanoparticles were evident in the nanocomposite as shown in Fig. 4(c) and (d).

3.2. Tensile properties

Fig. 7 shows yield strength (σ_{YS}, 0.2% proof stress), ultimate tensile strength (σ_{UTS}, the ultimate tensile strength) and elongation to fracture of the as-cast AZ91 alloy and SiCp/AZ91 nanocomposites. It can be seen from Fig. 7 that the ultimate tensile strength, yield strength of the SiCp/AZ91 nanocomposites are simultaneously enhanced compared with that of the as-cast AZ91 alloy. The elongation to fracture of the SiCp/AZ91 nanocomposite stirring for 5 min even exhibits significant improvement compared with the as-cast AZ91 alloy. This is very different from what is observed in the magnesium matrix composite using traditional reinforcements such as micro-sized particles and fibers. However, with increasing the stirring time, the ultimate tensile strength and elongation to fracture of the SiCp/AZ91 nanocomposites decrease.

According to the classic Hall–Petch equation: $\sigma_y = \sigma_0 + K_y d^{-1/2}$, where σ_y is the yield strength, σ_0 and K_y are material constants, and d is the mean grain size. The value of K_y is dependent on the number of slip systems. It is higher for HCP metals than for FCC and BCC metals [25]. Since Mg is HCP, the grain size affects the yield strength significantly. As shown in Figs. 3(a) and 4(a), the phase $Mg_{17}Al_{12}$ in the as-cast AZ91 alloy constitutes a continuous brittle phase along the grain boundaries of α-Mg dendrites which decreases the tensile strength. With the addition of SiC nanoparticles, more grain boundaries associated with finer α-Mg grains in the SiCp/AZ91 nanocomposites would obviously result in the

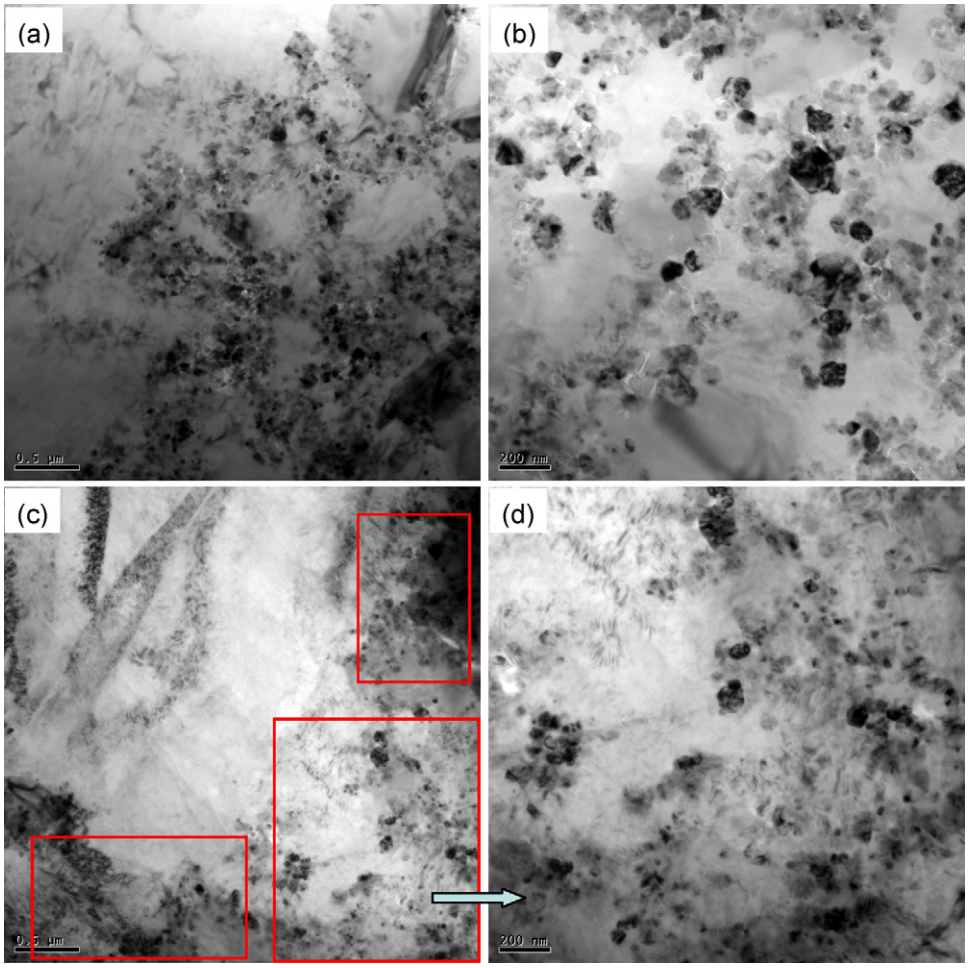

Fig. 6. TEM micrographs of SiCp/AZ91 nanocomposites: low magnification of SiC nanoparticles (a) stirring for 5 min; (c) stirring for 10 min; higher magnification of SiC nanoparticles (b) stirring for 5 min; (d) stirring for 10 min.

improvement of yield strength. Most of the phase $Mg_{17}Al_{12}$ in the SiCp/AZ91 nanocomposite stirring for 5 min varies from massive to lamellar as shown in Figs. 3(b) and 4(b), which will contribute to the improvement of the tensile strength as well. With increasing the stirring time, amount of the refined phase $Mg_{17}Al_{12}$ along the grain boundaries decreases while agglomerates of SiC nanoparticles increase (Figs. 3 and 4), which would impair the tensile strength. Thus, it is thought that discontinuity and refinement of the phase $Mg_{17}Al_{12}$, the refinement of α-Mg grains and the addition of the SiC nanoparticles should play a major role in enhancement of the tensile properties of the nanocomposite in our work as shown in Fig. 7.

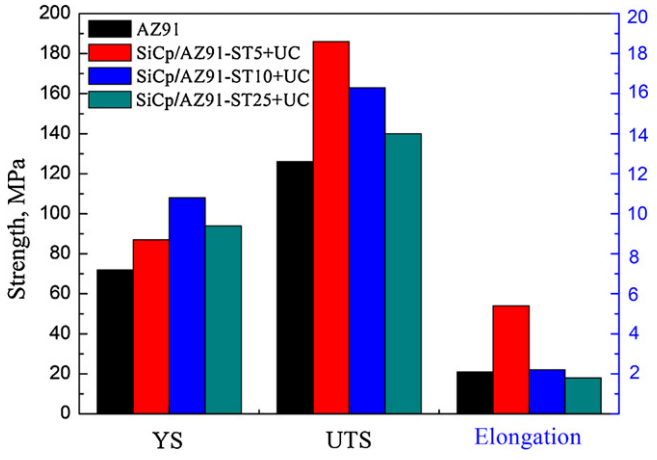

Fig. 7. Tensile strength of AZ91 alloy and SiCp/AZ91 nanocomposites.

4. Conclusions

The microstructure and mechanical properties of SiCp/AZ91 nanocomposites prepared with semisolid stirring assisted ultrasonic vibration are experimentally investigated.

(1) The grains of matrix alloy in the SiCp/AZ91 nanocomposite are refined compared with the as-cast AZ91 alloy. With increasing the stirring time the grain size of matrix alloy exhibits negligible change.
(2) Although some SiC nanoparticle clusters still exist along the grain boundary, the SiC nanoparticles disperse uniformly outside the SiC nanoparticle clusters. With increasing the stirring time, agglomerates of SiC nanoparticles increase.
(3) The ultimate tensile strength, yield strength and elongation to fracture of the SiCp/AZ91 nanocomposite stirring for 5 min are simultaneously enhanced compared with the as-cast AZ91 alloy. With increasing the stirring time, ultimate tensile strength and elongation to fracture of the SiCp/AZ91 nanocomposite decrease.

Acknowledgments

This work was supported by "the Fundamental Research Funds for the Central Universities" (Grant No. HIT.NSRIF.201130).

References

[1] M. Gupta, M.O. Lai, D. Saravanaranganathan, J. Mater. Sci. 35 (2000) 2155–2165.
[2] S.F. Hassan, M. Gupta, J. Mater. Sci. 37 (2002) 2467–2474.
[3] B.L. Mordike, T. Ebert, Mater. Sci. Eng. A 302 (2001) 37–45.
[4] Y. Morisada, H. Fujii, T. Nagaoka, M. Fukusumi, Scripta Mater. 55 (2006) 1067–1070.
[5] R. Gehrmann, M.M. Frommert, G. Gottstein, Mater. Sci. Eng. A 395 (2005) 338–349.
[6] S.F. Hassan, M. Gupta, J. Alloys Compd. 429 (2007) 176–183.
[7] Q.B. Nguyen, M. Gupta, J. Alloys Compd. 490 (2010) 382–387.
[8] S.F. Hassan, K.S. Tun, M. Gupta, J. Alloys Compd. 509 (2011) 4341–4347.
[9] C.S. Goh, J. Wei, L.C. Lee, M. Gupta, Acta Mater. 55 (2007) 5115–5121.
[10] S.F. Hassan, M. Gupta, Metall. Mater. Trans. A 36 (2005) 2253–2258.
[11] S. Sankaranarayanan, S. Jayalakshmi, M. Gupta, J. Alloys Compd. (2010), doi:10.1016/j.jallcom.2011.04.083.
[12] C.S. Goh, M. Gupta, J. Wei, L.C. Lee, J. Compos. Mater. 41 (2007) 2325–2335.
[13] C.J. Lee, J.C. Huang, P.J. Hsieh, Scripta Mater. 54 (2006) 1415–1420.
[14] H.C. Zhong, H. Wang, L.Z. Ouyang, M. Zhu, J. Alloys Compd. 509 (2011) 4268–4272.
[15] J. Lan, Y. Yang, X. Li, Mater. Sci. Eng. A 386 (2004) 284–290.
[16] Y. Yang, J. Lan, X. Li, Mater. Sci. Eng. A 380 (2004) 378–383.
[17] G. Cao, H. Konishi, X. Li, Mater. Sci. Eng. A 486 (2009) 357–362.
[18] J.S.C. Jang, L.J. Chang, J.H. Young, J.C. Huang, C.Y.A. Tsao, Intermetallics 14 (2006) 945–950.
[19] K.S. Suslick, Annu. Rev. Mater. Sci. 29 (1999) 295–326.
[20] M. Khosro Aghayani, B. Niroumand, J. Alloys Compd. 509 (2011) 114–122.
[21] X. Liu, Y. Osawa, S. Takamori, T. Mukai, Mater. Lett. 62 (2008) 2872–2875.
[22] X. Liu, Y. Osawa, S. Takamori, T. Mukai, Mater. Sci. Eng. A 487 (2008) 120–123.
[23] A. Luo, Scripta Metall. Mater. 31 (1993) 1253–1258.
[24] X.J. Wang, K. Wu, W.X. Huang, H.F. Zhang, M.Y. Zheng, D.L. Peng, Compos. Sci. Technol. 67 (2007) 2253–2260.
[25] H.Z. Ye, X.Y. Liu, J. Mater. Sci. 39 (2004) 6153–6171.